**T. F. Lemczyk**
Research Engineer.

**B. L. Mack**
Research Engineer.

**J. R. Culham**
Assistant Director.

**M. M. Yovanovich**
Professor of Mechanical Engineering,
Director, MHTL.

Microelectronics Heat Transfer Laboratory,
University of Waterloo,
Waterloo, Ontario, Canada N2L 3G1

# PCB Trace Thermal Analysis and Effective Conductivity

*The electrical current carrying capability of a surface or buried trace located within a fiberglass printed circuit board (PCB), is of important interest in the microelectronics industry. The maximum allowable trace power, hence local integrity and maximum allowable operating temperature, will depend on several parameters including the circuit board thermal conductivity, thickness, trace size and location. A two-dimensional, steady-state thermal conduction analysis is made on a finite, plane homogeneous medium (PCB), to examine the trace behavior. The trace is modeled as a zero-thickness, strip heat source with specified uniform temperature, and it's position in the medium is varied. A two-dimensional thermal analysis is also performed on a multilayered cell model with finite heat source, to establish an accurate, effective thermal conductivity for a typical PCB. Results are tabulated and presented graphically for both the two-dimensional trace and effective conductivity models.*

## Introduction

A typical printed circuit board (PCB) used in the microelectronics industry is constructed of alternating fiberglass and copper layers, as shown in Fig. 1(*a*). In the case of single-sided boards, attached to their top surface are the various electronic components. The components can be surface mounted or have pins that penetrate the board to a specific copper landing. The heat generated within an electronic package is dissipated to the fluid and to the PCB. The thermal resistance of the PCB then becomes part of the analysis to accurately estimate the chip die temperature.

The conduction problem associated with the heat flow through the PCB has been investigated by numerous researchers. The PCB is generally treated as composed of uniform, homogeneous multiple layers which occupy the entire dimensions of the PCB domain. By assuming an approximate effective thermal conductivity for the multiple layered system, the PCB can be modelled as a single homogeneous medium, with considerable savings in computational effort and time.

This work will focus on two specific aspects of PCB thermal analysis. First, an examination into trace thermal behavior will be conducted, whereby the trace is surface mounted or buried in the domain exposed to uniform cooling conditions over the PCB trace cell. The trace temperature rise can limit the electrical current that can run through a trace. By fixing the temperature of the trace to the maximum allowable operating temperature of the substrate medium, the total heat flow can be determined over a range of geometric parameters. The trace represents a finite-sized copper strip, as shown in Fig. 1(*b*), which is actually more realistic than a uniform copper layer across the board. Due to etching, the copper layers occupy only finite-strip locations, i.e., traces, within the PCB. A single trace will be examined, having a specified uniform temperature. This should give the designer a guideline as to placement of the copper layers (i.e., traces) within or on the surface of a PCB.

A second examination is conducted into establishing an effective thermal conductivity for a multilayered PCB. Previous work of this nature has usually assumed a series or parallel thermal resistance analysis, to obtain a well known conductivity expression. Although this will not provide very good agreement in temperature levels across the PCB, and especially at a heat source, it will be shown that the mean heat source

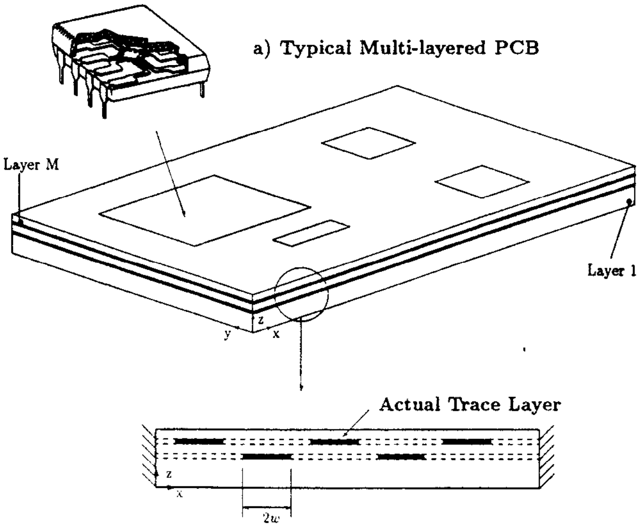

a) Typical Multi-layered PCB

b) Trace Location Within The PCB

Fig. 1 Trace location in a PCB

---

Contributed by the Electrical and Electronic Packaging Division for publication in the JOURNAL OF ELECTRONIC PACKAGING. Manuscript received by the EEPD January 29, 1991; revised manuscript received September 9, 1992. Associate Technical Editor: W. Z. Black.

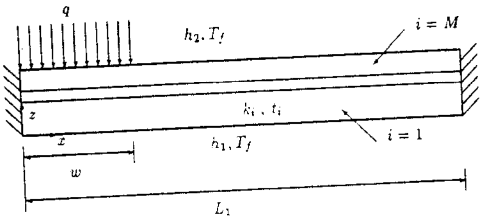

Fig. 2 Multilayered 2-D PCB model

temperature, hence PCB thermal resistance, can be closely estimated. Since many typical circuit boards are composed of three or more individual layers of alternating fiberglass and copper, the simulation advantages are again clear from a computational viewpoint.

All analyses in this work will use a separable Fourier series solution to the conduction problem. Other numerical procedures could have been used, but the simple analytical approach chosen has proven accurate and reliable in many previous studies (Negus and Yovanovich, 1986; Lemczyk et al., 1988; Lemczyk et al., 1989) and allows for easy and accurate implementation on a personal computer.

## Two-Dimensional Analysis

Before commencing the individual analysis of the 2-D trace and effective conductivity models discussed, we will introduce some general equations and relations needed for all solutions. The multilayered effective conductivity system shown in Fig. 2, will be used as a basis for reference.

From Fig. 2, we consider a general multi-layered board where in each layer,

$$\nabla^2 T_i = 0 \tag{1}$$

and a homogeneous thermal conductivity, $k_i$, is assumed. The local coordinate system, $x$, $z$, of each layer is located at the bottom left corner as illustrated, for each layer.

For steady-state, two-dimensional heat conduction, a separable Fourier series solution for $T_i - T_f \equiv T_i(x, z)$, can be obtained straightforwardly,

$$T_i(x, z) = \sum_{n=0}^{\infty} \cos(\lambda_n x/L_1)[a_{i,n}\alpha_n(z) + b_{i,n}\beta_n(z)] \tag{2}$$

where

$$\alpha_n(z) = \cosh(\lambda_n z/L_1), \; n = 0, 1, 2, \ldots; \tag{3}$$

$$\beta_n(z) = \sinh(\lambda_n z/L_1), \; n = 1, 2, 3, \ldots; \; \beta_0(z) = z \tag{4}$$

and this satisfies the insulated end conditions ($\partial T/\partial x = 0$) for each layer at $x = 0$, $L_1$, with

$$\lambda_n = n\pi \tag{5}$$

For multiple layers, the layers are perfectly attached to each other, thus satisfying along the whole of each interface,

$$T_i(x, t_i) = T_{i+1}(x, 0) \tag{6}$$

$$\kappa_i \frac{\partial T_i}{\partial z}(x, t_i) = \frac{\partial T_{i+1}}{\partial z}(x, 0) \tag{7}$$

where

$$\kappa_i = \frac{k_i}{k_{i+1}} \tag{8}$$

Using orthogonality, the constants in Eq. (2) may be related to each other using Eqs. (6) and (7), and it can be shown that in proceeding from layer $i = 1$ to layer $i = M$,

$$a_{i+1,n} = a_{i,n}\cosh(\lambda_n t_i/L_1) + b_{i,n}\sinh(\lambda_n t_i/L_1), \; n = 1, 2, 3, \ldots \tag{9}$$

$$b_{i+1,n} = \kappa_i(a_{i,n}\sinh(\lambda_n t_i/L_1) + b_{i,n}\cosh(\lambda_n t_i/L_1)), \; n = 1, 2, 3, \ldots \tag{10}$$

$$a_{i+1,0} = a_{i,0} + b_{i,0}t_i \tag{11}$$

$$b_{i+1,0} = \kappa_i b_{i,0} \tag{12}$$

The bottom surface of the system ($z = 0$ of layer $i = 1$) is exposed to a uniform convective boundary condition

$$L_1 \frac{\partial T_1}{\partial z} - Bi_1 T_1 = 0; \quad z = 0, \; 0 \le x \le L_1; \quad Bi_1 = \frac{h_1 L_1}{k_1} \tag{13}$$

which easily yields

$$b_{1,n} = g_n a_{1,n} \tag{14}$$

where

$$g_n = \frac{Bi_1}{\lambda_n}, \; n = 1, 2, 3, \ldots; \quad g_0 = \frac{Bi_1}{L_1} \tag{15}$$

A general form for the expansion of $T_M(x, t_M)$ can be obtained,

$$T_M(x, t_M) = \sum_{n=0}^{\infty} a_{1,n}\phi_M(n, t_M)\cos(\lambda_n x/L_1) \tag{16}$$

and also for the temperature gradient, at $z = t_M$,

## Nomenclature

$a_{i,n}, b_{i,n}$ = Fourier series coefficients for each layer $i$
$A_{k,n}$ = symmetric solution matrix $[N + 1]$ for Fourier coefficients
$Bi_1, Bi_2$ = dimensionless Biot numbers
$c_n$ = approximate Fourier series coefficients in minimization solution
$f_{1,n}, f_{2,n}$ = recursive multilayer functions in Fourier series solution
$F$ = quadratic functional for Fourier coefficient solution
$g_n$ = relational coefficient
$h_1, h_2$ = surface convection film coefficients, W/m$^2$K
$k_H, k_P, k_S$ = effective harmonic-mean parallel and series thermal conductivities, W/mK
$k_i$ = thermal conductivity for each $i$-layer, W/mK
$L_1, L_2$ = system dimensions: length and width, m
$N$ = Fourier series truncation value
$q, q_s$ = specified system heat flux for effective conductivity models, W/m$^2$
$Q_a, Q_b, Q_c, Q_d$ = total heat flow for trace model cases ($a$) to ($d$), W
$R_a, R_b, R_c, R_d$ = thermal resistances for trace model cases ($a$) to ($d$), °C/W
$T_c$ = trace model contact temperature $\equiv T - T_f$, °C
$t_i$ = $i$-layer thickness in $z$-direction, m
$T_f$ = ambient (fluid) temperature, °C
$T_i$ = two-dimensional steady-state temperature field in each layer $i$, °C
$w$ = heat source contact length, m
$x, y, z$ = Cartesian coordinates
$\alpha_n, \beta_n$ = hyperbolic functions for Fourier solution
$\kappa_i$ = thermal conductivity ratio $\equiv k_i/k_{i+1}$
$\lambda_n$ = Fourier characteristic roots
$\phi, \phi'$ = Fourier series function, derivative of
$\Psi_{a,b,c,d}$ = dimensionless thermal resistance factors for trace model cases ($a$) to ($d$)

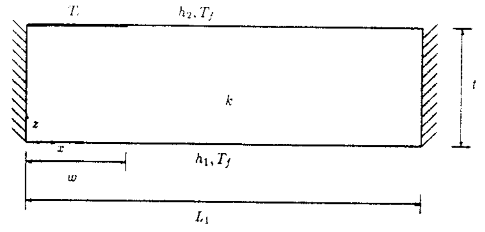

a) Surface Trace Model

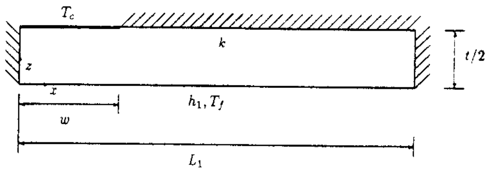

b) Mid-Buried Trace Model

Fig. 3 2-D trace models

$$\frac{\partial T_M}{\partial z}(x, t_M) = \sum_{n=0}^{\infty} a_{1,n}\phi_M'(n, t_M)\cos(\lambda_n x/L_1) \tag{17}$$

with

$$\phi_M(n, z) = f_{1,n}\alpha_n(z) + f_{2,n}\beta_n(z),\ n = 0, 1, 2, \ldots \tag{18}$$

The derivative function $\phi_M'$ is obtained by differentiating with respect to $z$. For $i = 1$, the $f_{1,n}, f_{2,n}$ functions are defined by

$$f_{1,n} = 1, f_{2,n} = g_n, f_{1,0} = 1, f_{2,0} = g_0 \tag{19}$$

These are recursively defined if $i > 1$ using the above as initial values, and Eqs. (9) to (12). This procedure is summarized in Lemczyk et al. (1988).

**2-D Effective Conductivity Model.** Using the above solutions, the multi-layered system in Fig. 2 has the remaining boundary conditions to be satisfied on $z = t_M$ of layer $i = M$:

$$\frac{\partial T_M}{\partial z} = \frac{q}{k_M};\quad z = t_M;\quad 0 \le x \le w; \tag{20}$$

$$L_1\frac{\partial T_M}{\partial z} + Bi_2 T_M = 0;\quad z = t_M;\quad w \le x \le L_1;\quad Bi_2 = \frac{h_2 L_1}{k_M} \tag{21}$$

Using these equations, we can define the quadratic functional form using Eqs. (16) and (17)

$$F = \int_0^{L_1}\left[\sum_{n=0}^{N} c_n\psi_n(x) - r(x)\right]^2 dx \tag{22}$$

and minimizing this with respect to $c_n$, (i.e., setting $\partial F/\partial c_k = 0$), we can obtain a symmetric set of $N + 1$ linear equations

$$[A_{k,n}]c_n = r_k \tag{23}$$

for the approximate solution of the unknown $c_n$, which are expressed in terms of the $a_{1,n}$. Using Eqs. (20) to (22), the entries of $[A_{k,n}]$, $r_k$ are given in detail in Lemczyk and Culham (1989).

**2-D Trace Model.** The systems shown in Fig. 3 represent the two-dimensional trace models to be studied. The substrate is a single homogeneous medium with thermal conductivity, $k$. Figure 3($a$) shows the basic thermal cell for modelling the trace. The trace (contact) temperature $T_c$ will be fixed for all cases. Four cases will be considered which give insight into the thermal resistance behavior and heat flow rate of the trace model.

The approximate solution of the temperature field in Eq. (16) will involve the minimization of the quadratic functional for the Fourier series to obtain the necessary coefficients $c_n$. This will be defined for all cases as

$$F = \int_0^{w}\left[\sum_{n=0}^{N} c_n\psi_{n,1}(x) - r_1(x)\right]^2 dx + \int_w^{L_1}\left[\sum_{n=0}^{N} c_n\psi_{n,2}(x) - r_2(x)\right]^2 dx \tag{24}$$

The $z$-location and particular functions $\psi_n$, $r$ can be established from the specific boundary conditions below. These are outlined in detail in Lemczyk (1990).

**Case (a).** The trace is located on the top surface ($z = t$) of the model in Fig. 3($a$). Also, $h_1 = h_2 > 0$. Using Eq. (16) which satisfies Eq. (13), the remaining boundary conditions become

$$T = T_c;\quad z = t;\quad 0 \le x \le w; \tag{25}$$

$$L_1\frac{\partial T}{\partial z} + Bi_2 T = 0;\quad z = t;\quad w \le x \le L_1;\quad Bi_2 = \frac{h_2 L_1}{k} \tag{26}$$

The total heat flow rate and thermal resistance will be defined as

$$Q_a = kL_2T_c\left(Bi_2\frac{w}{L_1} + \frac{q_s}{T_c}\right) \tag{27}$$

$$R_a = \frac{T_c}{Q_a} \tag{28}$$

with

$$q_s = a_{1,0}\phi_0'(t)w + L_1\sum_{n=1}^{N} a_{1,n}\phi_n'(t)\sin(\lambda_n w/L_1)/\lambda_n \tag{29}$$

The form for $Q_a$ reflects the fact that there is convective cooling with $h_2$ over the range $0 \le x \le L_1$ even though the boundary condition in Eq. (26) only uses $w \le x \le L_1$. The total heat flow will be comprised of the sum of heat entering the solid and leaving through the fluid film coefficient over the contact zone $0 < x \le w$.

**Case (b).** By locating the trace mid-way at $z = t/2$ of the cell model in Fig. 3($a$), and maintaining $h_1 = h_2$, the resulting analysis can be performed on a symmetric half-cell as shown in Fig. 3($b$). The resulting total resistance will thus be one-half that for the system in Fig. 3($b$). Therefore, Eq. (16) can be used with the boundary conditions

$$T = T_c;\quad z = t/2;\quad 0 \le x \le w \tag{30}$$

$$\frac{\partial T}{\partial z} = 0;\quad z = t/2;\quad w \le x \le L_1 \tag{31}$$

$Q_b$ and $R_b$ will reflect the total system values, i.e., two of these half-cells, hence

$$Q_b = 2kL_2q_s \tag{32}$$

$$R_b = \frac{T_c}{Q_b} \tag{33}$$

where $q_s$ is of the same form as Eq. (29).

**Case (c).** By setting $h_1 = 0$, and leaving the trace on the surface $z = t$ as in Fig. 3($a$), gives $Q_c$, $R_c$ of the same form as $Q_a$, $R_a$ in Eqs. (27) and (28).

**Case (d).** With $h_1 = 0$, and placing the trace at $z = 0$, the analysis is identical to using the system shown in Fig. 3($b$) (i.e., a mirror image), with total thickness $t$, and identifying $h_2 = 0$ instead.

In this case we get

Table 1 Polyamide and FR4 trace comparisons

| $w$ [μm] | $t$ [μm] | $L_1$ [μm] | $Q_a$ [W] | $Q_b$ [W] | $Q_c$ [W] | $Q_d$ [W] | $R_a$ [°C/W] | $R_b$ [°C/W] | $R_c$ [°C/W] | $R_d$ [°C/W] |
|---|---|---|---|---|---|---|---|---|---|---|
| | | | | | | | | | ($\times 10^2$) | |
| Polyamide $k$ = 0.2 W/mK | | | | | | | | | | |
| 10 | 10 | 20 | .036 | .036 | .036 | .018 | 25.0 | 25.0 | 25.0 | 50.0 |
| 10 | 50 | 20 | .036 | .036 | .036 | .018 | 25.0 | 25.0 | 25.0 | 50.1 |
| 10 | 10 | 50 | .089 | .090 | .063 | .045 | 10.1 | 10.1 | 14.4 | 20.1 |
| 10 | 50 | 50 | .090 | .090 | .063 | .045 | 10.1 | 10.0 | 14.3 | 20.1 |
| 50 | 50 | 100 | 0.179 | .179 | .108 | .090 | 5.02 | 5.01 | 8.35 | 10.0 |
| 50 | 100 | 100 | .179 | .179 | .108 | .090 | 5.02 | 5.02 | 8.35 | 10.1 |
| 50 | 50 | 250 | .436 | .438 | .239 | .221 | 2.06 | 2.05 | 3.77 | 4.07 |
| 50 | 100 | 250 | .439 | .442 | .240 | .221 | 2.05 | 2.04 | 3.75 | 4.06 |
| FR-4 $k = 0.4$ W/mK | | | | | | | | | | |
| 50 | 1000 | 100 | .178 | .178 | .126 | .088 | 5.07 | 5.07 | 7.17 | 10.3 |
| 50 | 2000 | 100 | .176 | .175 | .125 | .086 | 5.13 | 5.13 | 7.19 | 10.5 |
| 50 | 1000 | 250 | .440 | .442 | .259 | .218 | 2.04 | 2.04 | 3.47 | 4.12 |
| 50 | 2000 | 250 | .435 | .435 | .259 | .213 | 2.07 | 2.06 | 3.47 | 4.22 |
| 250 | 1000 | 500 | .884 | .886 | .484 | .438 | 1.02 | 1.02 | 1.86 | 2.07 |
| 250 | 2000 | 500 | .884 | .886 | .484 | .438 | 1.02 | 1.02 | 1.86 | 2.06 |
| 250 | 1000 | 1250 | 2.12 | 2.16 | 1.13 | 1.07 | .424 | .416 | .795 | .840 |
| 250 | 2000 | 1250 | 2.10 | 2.14 | 1.13 | 1.05 | .429 | .420 | .794 | .859 |

Table 2 Trace comparisons for $Bi_2 \leq 0.1$

| $Bi_2$ | $t/L_1$ | $w/L_1$ | $\Psi_a$ | $\Psi_b$ | $\Psi_c$ | $\Psi_d$ |
|---|---|---|---|---|---|---|
| | | | | $\times 10^3$ | | |
| 0.001 | .01 | 0.1 | .5284 | .5332 | .5284 | 1.032 |
| 0.001 | .01 | 1.0 | .5000 | .5000 | .5000 | 1.000 |
| 0.001 | 1. | 0.1 | .5018 | .5012 | .5018 | 1.003 |
| 0.001 | 1. | 1.0 | .5002 | .5002 | .5002 | 1.001 |
| 0.001 | 10. | 0.1 | .5040 | .5034 | .5040 | 1.012 |
| 0.001 | 10. | 1.0 | .5025 | .5025 | .5025 | 1.010 |
| | | | | $\times 10^2$ | | |
| 0.01 | .01 | 0.1 | .7210 | .7226 | 1.147 | 1.240 |
| 0.01 | .01 | 1.0 | .5000 | .5000 | .9091 | 1.000 |
| 0.01 | 1.0 | 0.1 | .5150 | .5092 | .9219 | 1.023 |
| 0.01 | 1.0 | 1.0 | .5025 | .5025 | .9092 | 1.010 |
| 0.01 | 10. | 0.1 | .5363 | .5314 | .9226 | 1.113 |
| 0.01 | 10. | 1.0 | .5238 | .5250 | .9099 | 1.100 |
| | | | | $-10^1$ | | |
| 0.1 | .01 | 0.1 | 1.604 | 1.594 | 2.470 | 2.488 |
| 0.1 | .01 | 1.0 | .5002 | .5002 | .9901 | 1.001 |
| 0.1 | 1. | 0.1 | .6441 | .5891 | 1.111 | 1.223 |
| 0.1 | 1. | 1.0 | .5238 | .5250 | .9901 | 1.100 |
| 0.1 | 10. | 0.1 | .7868 | .8116 | 1.111 | 2.123 |
| 0.1 | 10. | 1.0 | .6667 | .7500 | .9902 | 2.000 |

Table 3 Trace comparisons for $Bi_2 \geq 1.0$

| $Bi_2$ | $t/L_1$ | $w/L_1$ | $\Psi_a$ | $\Psi_b$ | $\Psi_c$ | $\Psi_d$ |
|---|---|---|---|---|---|---|
| | | | | $\times 10^1$ | | |
| 1.0 | .01 | 0.1 | .3155 | .3112 | .5296 | .5355 |
| 1.0 | .01 | 1.0 | .0503 | .0503 | .1000 | 1.010 |
| 1.0 | 1. | 0.1 | .1686 | .1377 | .2018 | .3227 |
| 1.0 | 1. | 1.0 | .6667 | .7500 | .9990 | .2000 |
| 1.0 | 10. | 0.1 | .1935 | .3614 | .2017 | 1.223 |
| 1.0 | 10. | 1.0 | .0917 | .3000 | .1000 | 1.100 |
| | | | | $\times 10^1$ | | |
| 10.0 | .01 | 0.1 | .0461 | .0465 | .0813 | .0913 |
| 10.0 | .01 | 1.0 | .0052 | .0053 | .0100 | .0110 |
| 10.0 | 1. | 0.1 | .0538 | .0900 | .0546 | .2325 |
| 10.0 | 1. | 1.0 | .0092 | .0300 | .0100 | .1100 |
| 10.0 | 10. | 0.1 | .0545 | .3163 | .0546 | 1.133 |
| 10.0 | 10. | 1.0 | .0099 | .2550 | .0100 | 1.010 |
| | | | | $\times 10^{-1}$ | | |
| 100. | .01 | 0.1 | .6550 | .7809 | .9567 | 2.014 |
| 100. | .01 | 1.0 | .0667 | .0750 | .1000 | .2000 |
| 100. | 1. | 0.1 | .8882 | 8.444 | .8892 | 22.34 |
| 100. | 1. | 1.0 | .0990 | 2.550 | .1000 | 10.10 |
| 100. | 10. | 0.1 | .8891 | 31.18 | .8892 | 112.4 |
| 100. | 10. | 1.0 | .0999 | 25.05 | .1000 | 100.1 |

$$Q_d = kL_2 q_s \tag{34}$$

$$R_d = \frac{T_c}{Q_d} \tag{35}$$

A dimensionless thermal resistance factor will be defined for all cases (*a*) to (*d*) as

$$\Psi = kL_2 R \tag{36}$$

## Trace Results

Table 1 shows the dimensional results for two specific substrate materials, namely polyamide and fiberglass (FR4). Polyamide is a polymer material being used in the construction of special microelectronic components, and fiberglass is a typical PCB material. The maximum operating temperature was taken as 110°C for each material. Setting $T_f$ = 20°C, hence the contact temperature becomes $T_c$ = 90°C using the temperature difference definition for $T_i$. Over a wide range of geometry, with $L_2$ = 1 m, and setting $h_1 = h_2$ = 10 W/m$^2$K (approximate natural convection film coefficient), the results show that there is little sensitivity to placement of the trace on the surface (Case (*a*)) or mid-way through the medium (Case (*b*)), for either polyamide or fiberglass, if the top and bottom boundary conditions are similar.

It is important to note that for polyamide, the range of $Bi_2$ was $.001 \leq Bi_2 \leq .0125$, and for fiberglass $.0025 \leq Bi_2 \leq .03125$. When $h_1 = 0$, and the trace was placed on the top surface with convective cooling $h_2$ (Case (*c*)), or on the bottom surface (Case (*d*)), there was a difference in results. For polyamide, at $Bi_2$ = .001, there was a 100 percent gain in the allowable heat flow rate, i.e. twice the heat flow is possible with the top surface placement of the trace. For $Bi_2$ = .0125, a 9 percent increase is possible.

For fiberglass, at $Bi_2$ = .0025, a 43 percent increase in heat flow rate is possible with surface placement, and for $Bi_2$ = .03125, an 8 percent increase. In comparing Cases (*a*) or (*b*), with (*c*) or (*d*), it is clearly seen that a 100 percent increase in trace heat flow rate is possible if top and bottom surfaces are suitably exposed to a free stream. The trace optimization will not be a function of depth placement if both surfaces are suitably cooled. In the extreme limit, where one surface is assumed insulated, the optimal placement of the trace should obviously be on the exposed film surface.

A wider range of parameters were studied in dimensionless form for the trace cell Cases (*a*) to (*d*). Results are given in Tables 2 and 3 for $0.001 \leq Bi_2 \leq 100$, $0.01 \leq t/L_1 \leq 10$,

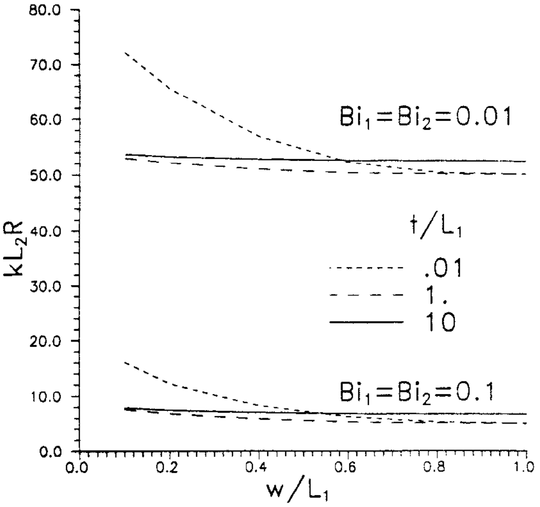

**Fig. 4** $\Psi_a$, $\Psi_b$ for $Bi_2$ = .01, .1

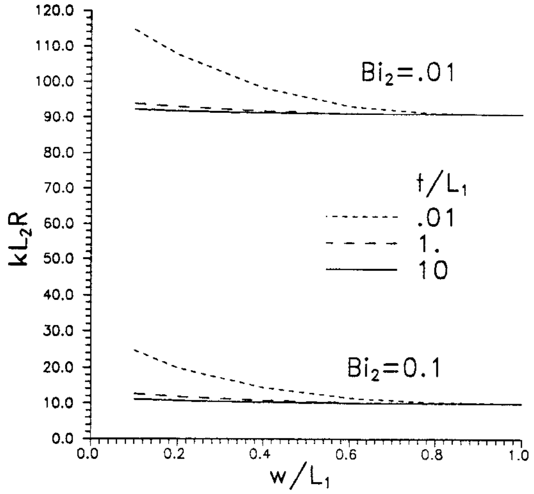

**Fig. 5** $\Psi_c$ for $Bi_2$ = .01, .1

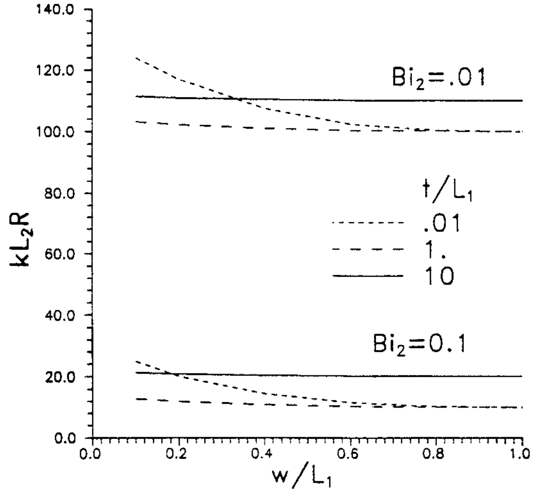

**Fig. 6** $\Psi_d$ for $Bi_2$ = .01, .1

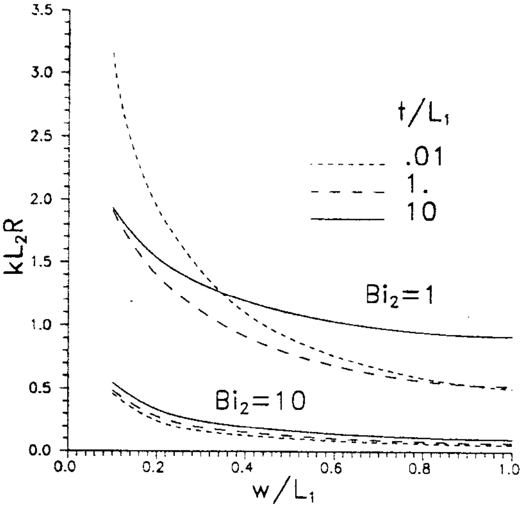

**Fig. 7** $\Psi_a$ for $Bi_2$ = 1, 10

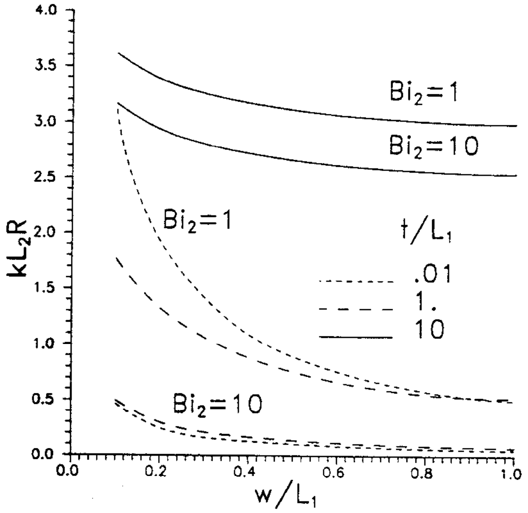

**Fig. 8** $\Psi_b$ for $Bi_2$ = 1, 10

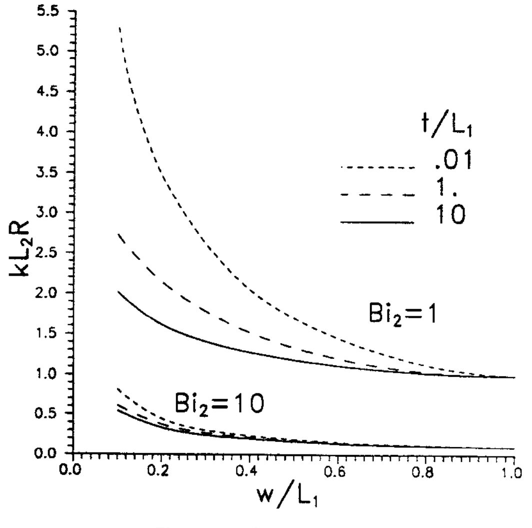

**Fig. 9** $\Psi_c$ for $Bi_2$ = 1, 10

$0.1 \leq w/L_1 \leq 1.0$. Results are also shown graphically in Figs. 4 to 10. For $Bi_2 \leq 0.1$, there is very little difference in results of trace depth placement if $h_1 = h_2 > 0$. Only for $Bi_2 \geq 1.0$, and $t/L_1 > 1$, does there appear a dependence on depth placement. For $Bi_2 \leq 0.1$ there will always be greater thermal resistance for Case ($c$) than ($a$) or ($b$), however for larger $Bi_2$ it becomes readily apparent that this trend will reverse itself (between ($b$) and ($c$) only) since the least resistance path is on the top surface.

## Effective Conductivity Results

Approximate parallel and series effective thermal conductivities for multilayered structures have often been used to

**Table 4 Thermal resistance comparisons for a 3-Layer PCB**

3 layer PCB; $k_S = 0.41$, $k_P = 9.12$, $k_H = 0.78$ W/mK

| $w/L_1$ | $R$ | $R_S$ | %Δ | $R_P$ | %Δ | $R_H$ | %Δ |
|---|---|---|---|---|---|---|---|
| 0.1 | 134.3 | 139.0 | 3.9 | 130.7 | −2.7 | 135.1 | 0.6 |
| 0.25 | 147.4 | 156.7 | 6.3 | 142.9 | −3.0 | 150.1 | 1.8 |
| 0.5 | 172.3 | 183.5 | 6.6 | 166.8 | −3.2 | 175.6 | 1.9 |
| 0.75 | 205.6 | 212.2 | 3.2 | 199.2 | −3.1 | 206.0 | 0.2 |
| 0.9 | 230.4 | 233.5 | 1.3 | 224.0 | −2.8 | 228.8 | −0.7 |
| 1.0 | 259.7 | 259.7 | 0.0 | 250.4 | −3.6 | 255.1 | −1.8 |

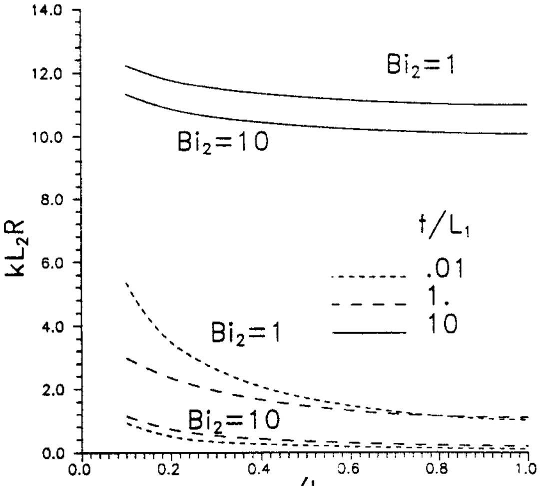

Fig. 10 $\Psi_d$ for $Bi_2$ = 1, 10

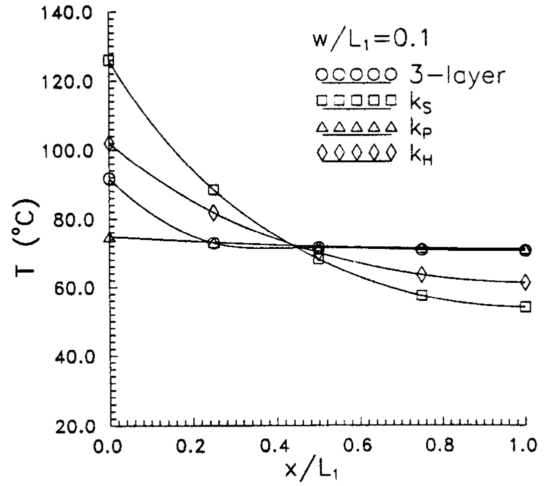

Fig. 11 3-layer PCB temperatures for $w/L_1$ = 0.1

model geometries close to the ideal parallel and series heat flow paths. For an M-layered PCB, for each layer having thickness $t_i$ and thermal conductivity, $k_i$, the formulas for these are:

$$k_P = \sum_{i=1}^{M} (k_i t_i) \Big/ \sum_{i=1}^{M} t_i \tag{37}$$

$$k_S = \sum_{i=1}^{M} t_i \Big/ \sum_{i=1}^{M} (t_i/k_i) \tag{38}$$

The specific objective of this study was to see how close an effective thermal conductivity, using a single homogeneous medium, can model an actual multilayered PCB. A conjugate heat flow model for PCB analysis, such as META outlined by Culham et al. (1990), uses a single one-dimensional homogeneous medium, thereby requiring some estimate for an effective

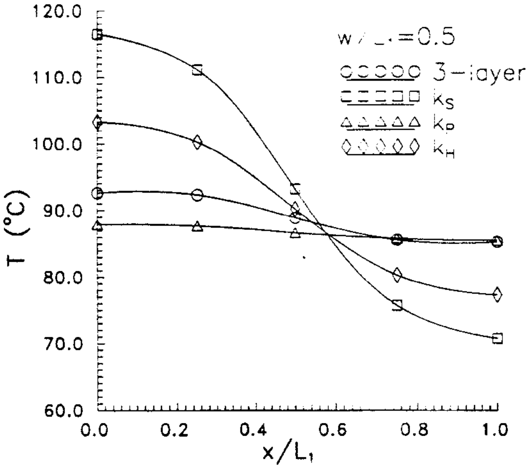

Fig. 12 3-layer PCB temperatures for $w/L_1$ = 0.5

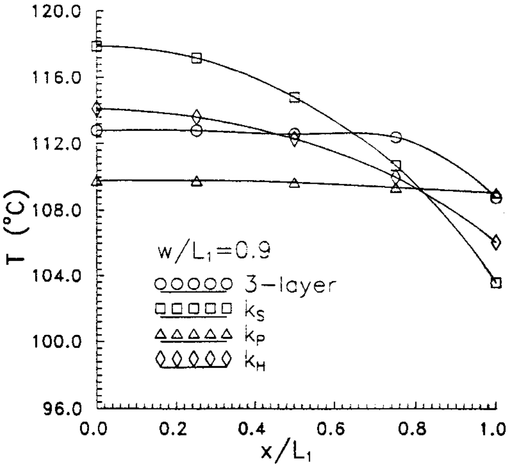

Fig. 13 3-layer PCB temperatures for $w/L_1$ = 0.9

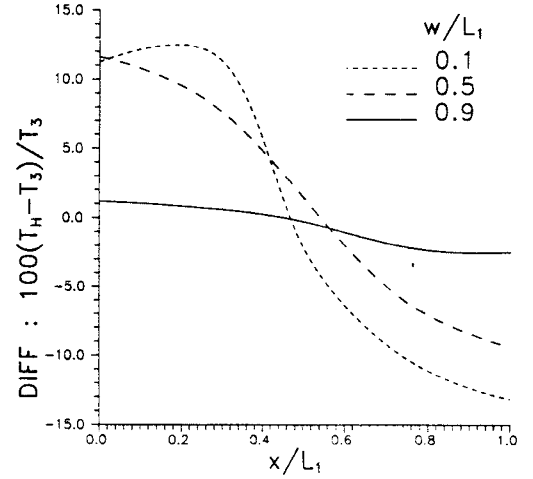

Fig. 14 Percent diff. in PCB temperatures as predicted by $k_H$

thermal conductivity. It was found that a harmonic-mean thermal conductivity, defined as

$$k_H^{-1} = \frac{1}{2}\left(\frac{1}{k_P} + \frac{1}{k_S}\right) \tag{39}$$

gave the best approximation to the PCB thermal resistance for the typical systems studied. A 3-layer PCB was modeled (refer to Fig. 2), having $t_1 = 7.78 \times 10^{-4}$ m, $k_1 = 0.4$ W/mK, $t_2 = 3.6 \times 10^{-5}$ m, $k_2 = 386$ W/mK, $t_3 = 7.78 \times 10^{-4}$ m, $k_3 = 0.4$ W/mK. These represent a layer of copper placed between two layers of fiberglass, the overall thickness being approx. 1.6 mm, a typical PCB thickness. A convection coefficient of $h = 10$ W/m$^2$K was used on the exposed surface, with $T_f = 20$°C, and the total heat flow rate was fixed at 0.4 W for all heat source sizes. The values of thermal resistance thereby directly reflect the mean temperature rise of the heat source contact. A range of $0.1 \le w/L_1 \le 1.0$ was studied; for resistance evaluations, $L_1 = 0.01$ m, $L_2 = 0.02$ m. The values of thermal resistance reported are twice the actual resistance for the cell in Fig. 2, i.e., representative of a full cell with trace width $2w$.

Results are shown in Table 4 and Figs. 11 to 14. Table 4 shows that for the full range of $w/L_1$, the harmonic-mean thermal conductivity $k_H$ will estimate the PCB thermal resistance to less than 2 percent. For $0.9 < w/L_1 \le 1.0$, the equivalent series thermal conductivity $k_S$ will give the most accurate estimate, since it is exact at $w/L_1 = 1.0$. Figures 11 to 13 illustrate that as $x/L_1 \rightarrow 1$, the parallel heat flow path is the most dominant, and therefore will estimate temperatures quite accurately in that region. However, on average, the harmonic-mean temperature solution appears to give the best representation. In these figures, the temperatures reported are on the top of layer 3 of the PCB. It is important to note that the range of percentage difference in actual temperatures over the PCB, as predicted by the harmonic-mean solution, is a bit greater than that reported for the resistances in Table 4. This is illustrated in Fig. 14.

## Conclusions

Results have been presented for two-dimensional trace modeling within a PCB, and for two-dimensional effective thermal conductivity studies on typical multiple layered PCBs. It can be concluded from the trace studies that little variation through depth placement was noticeable for the typical polyamide and fiberglass substrate materials.

An accurate expression for PCB effective thermal conductivity was obtained based on the harmonic mean of the equivalent parallel and series PCB conductivities. This can be used by single medium PCB codes, without need of discretizing through the PCB thickness to account for each individual layer. The computational savings are tremendous, especially since most PCB constructions comprise of three or more layers of copper and fiberglass. Although this will not give completely accurate temperature levels over the entire PCB, nonetheless the mean heat source temperature will be approximated quite accurately, as found to be within 2 percent, and this will give a very accurate prediction of the PCB thermal resistance, at considerable computational savings.

## Acknowledgments

The authors wish to acknowledge the financial support of the Natural Sciences and Engineering Research Council of Canada and to Bell Northern Research Ltd., Kanata, Canada, under CRD grant no. 661-062/88.

## References

Culham, J. R., and Yovanovich, M. M., 1987, "Non-Iterative Technique for Computing Temperature Distributions in Flat Plates with Distributed Heat Sources and Convective Cooling," presented at the 2nd ASME-JSME Thermal Engineering Joint Conference, Honolulu, Hawaii.

Culham, J. R., Lemczyk, T. F., Lee, S., and Yovanovich, M. M., 1990, "META—A Conjugate Heat Transfer Model for Air Cooling of Circuit Boards With Arbitrarily Located Heat Sources," submitted to the ASME JOURNAL OF ELECTRONIC PACKAGING.

Estes, R. C., 1989, "Thermal Characterization of Chip-on-Board Packaging Mechanisms," HTD-Vol. 111, *Heat Transfer in Electronics*, presented at the 1989 National Heat Transfer Conference.

Kraus, A. D., and Bar-Cohen, A., 1976, *Thermal Analysis and Control of Electronic Equipment*, McGraw-Hill, 4th Edition, New York.

Lemczyk, T. F., 1990, "PCB Trace Analysis and Effective Thermal Conductivity Studies," MHTL Report No. 9012 G-32, University of Waterloo MHTL.

Lemczyk, T. F., Culham, J. R., Yovanovich, M. M., 1988, "Two and Three-Dimensional, Multi-Layered Thermal Boards with Surface Heaters and Conjugate Fluid Flow," MHTL Report No. 8806 G-19, University of Waterloo MHTL.

Lemczyk, T. F., and Culham, J. R., 1989, *Thermal Analysis of Electronic Package Models*, MHTL Report No. 8903 G-27, University of Waterloo MHTL.

Lemczyk, T. F., Culham, J. R., and Yovanovich, M. M., 1989, "Analysis of Three-Dimensional Conjugate Heat Transfer Problems in Microelectronics," *Numerical Methods in Thermal Problems*, Vol. VI, Part 2, eds. R. W. Lewis and K. Morgan; part of the *Proceedings of the Sixth International Conference* held in Swansea, U.K., July 3–7.

Negus, K. J., and Yovanovich, M. M., 1986, "Thermal Analysis and Optimization of Convectively-Cooled Microelectronic Circuit Boards," *Heat Transfer in Electronic Equipment*, HTD-Vol. 57, presented at the AIAA/ASME 4th Thermophysics and Heat Transfer Conference, Boston, Mass., June 2–4.